ENGINEERING DEVELOPMENT OF SLURRY BUBBLE COLUMN REACTOR (SBCR) TECHNOLOGY

Quarterly Technical Progress Report No. 15

For the Period 1 October – 31 December 1998

FINAL

Contractor
AIR PRODUCTS AND CHEMICALS, INC.
7201 Hamilton Blvd.
Allentown, PA 18195-1501

Bernard A. Toseland, Ph.D.
Program Manager and Principal Investigator

Robert M. Kornosky
Contracting Officer's Representative

Prepared for the United States Department of Energy
Under Cooperative Agreement No. DE-FC22-95PC95051
Contract Period 3 April 1995 – 2 April 2000

NOTE: AIR PRODUCTS DOES NOT CONSIDER ANYTHING IN THIS REPORT TO BE CONFIDENTIAL OR PATENTABLE.

ENGINEERING DEVELOPMENT OF SLURRY BUBBLE COLUMN REACTOR (SBCR) TECHNOLOGY

Quarterly Technical Progress Report No. 15
For the Period 1 October – 31 December 1998

Contract Objectives

The major technical objectives of this program are threefold: 1) to develop the design tools and a fundamental understanding of the fluid dynamics of a slurry bubble column reactor to maximize reactor productivity, 2) to develop the mathematical reactor design models and gain an understanding of the hydrodynamic fundamentals under industrially relevant process conditions, and 3) to develop an understanding of the hydrodynamics and their interaction with the chemistries occurring in the bubble column reactor. Successful completion of these objectives will permit more efficient usage of the reactor column and tighter design criteria, increase overall reactor efficiency, and ensure a design that leads to stable reactor behavior when scaling up to large diameter reactors.

WASHINGTON UNIVERSITY IN ST. LOUIS

The report from Washington University for the period follows.

ENGINEERING DEVELOPMENT OF SLURRY BUBBLE COLUMN REACTOR (SBCR) TECHNOLOGY

Fifteenth Quarterly Report
for
October 1 - December 31, 1998

(Budget Year 4: October 1, 1998 – September 30, 1999)

Objectives for the Fourth Budget Year

The main goal of this subcontract from the Department of Energy via Air Products is to study the fluid dynamics of slurry bubble columns and address issues related to scaleup and design. The objectives set for the fourth budget year (October 1, 1998 – September 30, 1999) are listed below.

- Extension of CARPT/CT database to conditions of industrial interest such as high superficial gas velocity (up to 30-50 cm/s).
- Examination of the improved gas mixing phenomenological model against LaPorte tracer data.
- Critical evaluation of the developed phenomenological models for liquid and gas mixing against the newly obtained data.
- Testing of the 4-points optical probe for bubble sizes and bubble rise velocity measurements.
- Further improvement in Computational Fluid Dynamics (CFD) using CFDLIB and FLUENT through development of improved closure schemes and comparison of 2D and 3D model predictions with 2D and 3D data.

In this report, the research progress and achievements accomplished in the fifteenth quarter (October 1 - December 31, 1998) are summarized.

HIGHLIGHTS

Effect of the Distributor on Turbulent Kinetic Energy and Reynolds Shear Stress

Analysis of the effect of distributors on flow in bubble columns continues. In the September 1998 monthly report, we discussed the effect of the distributor on the overall gas holdup and time-averaged liquid recirculation velocity profiles. In this report, we examine the distributor effect on turbulent kinetic energy and Reynolds stress for the superficial gas velocity of 12 cm/s. The key findings were:

- The effect of the sparger on overall gas holdup diminished with an increase in superficial gas velocity and was marginal at a gas velocity of 12 cm/s.

- There was a pronounced distributor effect on the liquid recirculation velocity. The perforated plate distributor yielded a larger magnitude of time-averaged liquid recirculation velocities and a steeper axial velocity radial profile compared to the cone and bubble cup distributors. Similar time-averaged liquid velocity profiles were obtained using cone and bubble cup distributors.

- In the fully developed flow region, both the magnitude and shape of turbulent kinetic energy profiles were a function of the distributor type used, while the Reynolds stresses were not significantly affected by the distributor. Turbulent kinetic energies obtained with the cone and bubble cup distributors were larger than those obtained with the perforated plate distributor due to larger eddies.

- Larger bubble sizes were visually observed with the cone and bubble cup distributors compared to the perforated plate distributor. This supports the existence of larger eddies in columns with bubble and cone distributors.

- The differences in Reynolds shear stresses for the various distributors used were at most 10%, while larger Reynolds shear stresses were obtained with the perforated plate distributor compared to those obtained with the other two distributors. However, this difference was within the experimental error of the measurement.

The observations that the perforated plate distributor yielded a larger magnitude of liquid recirculation velocity and smaller turbulent kinetic energy need to be understood based on additional experiments for holdup profiles and bubble sizes and in the context of an appropriate hydrodynamic model.

Simulation of Gas-Liquid Flow in Cylindrical Bubble Columns with FLUENT: Comparison with CARPT-CT Experimental Results

- Validation of a transient, two-dimensional, axisymmetric simulation of a laboratory-scale cylindrical bubble column using the Fluent Library codes was attempted using the experimental data obtained in our laboratory by CARPT/CT at identical operating conditions. The simulation was performed using two different modeling approaches: i) the two-fluid Euler-Euler approach and ii) the algebraic slip mixture model approach. The two flow conditions selected from the available CARPT/CT data were i) bubbly flow regime at a superficial gas velocity of 2 cm/s and ii) churn-turbulent flow regime at a superficial gas velocity of 12 cm/s.

- Reasonably good agreement for the time-averaged mean axial liquid velocity profiles (measured via CARPT), as well as mean gas holdup profiles (measured via CT), were obtained from the simulations. Acceptable predictions of both the models at both the experimental conditions suggest robustness of the numerical techniques employed in FLUENT, and the validity of the assumptions of pseudo-homogeneity of phases, axisymmetry of the flow pattern and the closure equations used.

- Comparison of the experimentally measured mean turbulent energy profiles (via CARPT) and those from the simulation was good. This suggests that the two-dimensional simulation can indeed lead to predictions suitable for engineering calculations (not only of the mean profiles, but also of the second-order correlations), although the exact transient flow structures (which are non-axisymmetric) are missed because of the assumption of axisymmetry.

A detailed topical report that discusses the model equations and the results will follow.

1. EFFECT OF THE DISTRIBUTOR ON TURBULENT KINETIC ENERGY AND REYNOLDS SHEAR STRESS

In the 14th quarterly report (July 1 to September 30, 1998), we discussed the effect of the distributor on the overall gas holdup and time-averaged liquid recirculation velocity profiles. As mentioned at that time, some distributor effects were always observed in the entry region of the columns, but at higher gas velocities of about 12-15 cm/s, the effect of the distributor on holdup in the middle section of fully developed flow was marginal. However, a pronounced distributor effect on the liquid recirculation velocity (see Figure 1.1) was observed. In this report, we examine the distributor effect on turbulent kinetic energy and Reynolds stresses for the superficial gas velocity of 12 cm/s. In the fully developed region, both the magnitude and shape of turbulent kinetic energy profiles are a function of the distributor type used, while the distributor does not significantly affect the Reynolds stresses.

1.1 Effect of the Distributor on Turbulent Kinetic Energy

As shown in Figure 1.2, turbulent kinetic energy in the fully developed flow region obtained with the bubble cup and cone distributors is much larger than that obtained with the perforated plate distributor. The difference between centerline kinetic energies produced by the bubble cup or cone and perforated plate can be as much as 40%. This indicates that the bubble cup and cone distributors generate larger scale turbulence than does the perforated plate. These large eddies are more effectively recorded by the trace particle in CARPT, which can follow frequencies of up to 25 Hz. Whether this coarser scale of turbulence, apparent in the data for the cone and bubble cup distributor, is associated with larger scale bubbles produced by these two distributors is not certain at present. This will be investigated in the future with our four-point optical fiber probe.

1.2 Effect of the Distributor on Reynolds Shear Stress

As shown in Figure 1.3, there is no significant difference between the turbulent shear stresses for the cone and bubble cup distributor used. The perforated plate distributor gives slightly larger Reynolds shear stress values in the region between *r/R ~ 0.4 to r/R ~ 0.8* compared to those obtained by the other two distributors. The maximum difference is 10%.

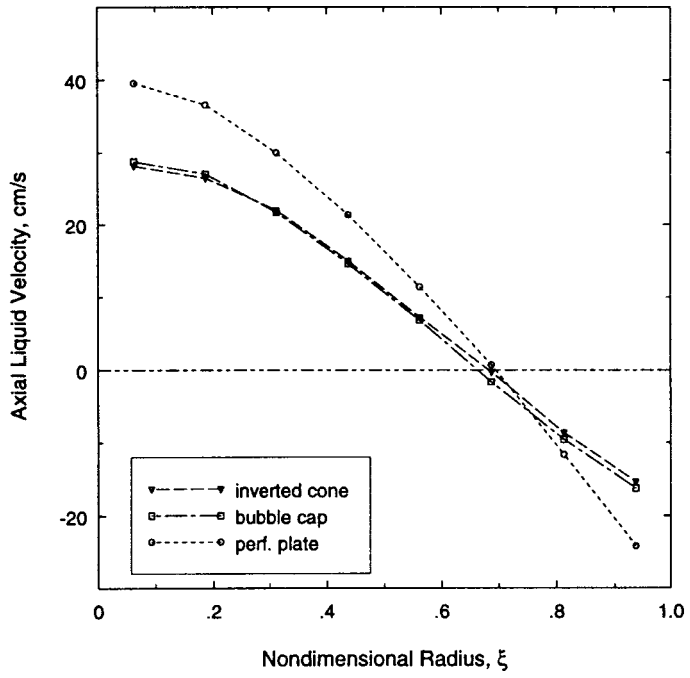

Figure 1.1 Effect of Distributor on the Time-Averaged Liquid Velocity in a 19-cm Diameter Column, *U*g = 12.0 cm/s. Distributors are cone (8C): one point inlet (1.27 cm in diameter); bubble cap (8B); perforated plate (8A): 0.33 mm hole diameter and 0.05% open area.

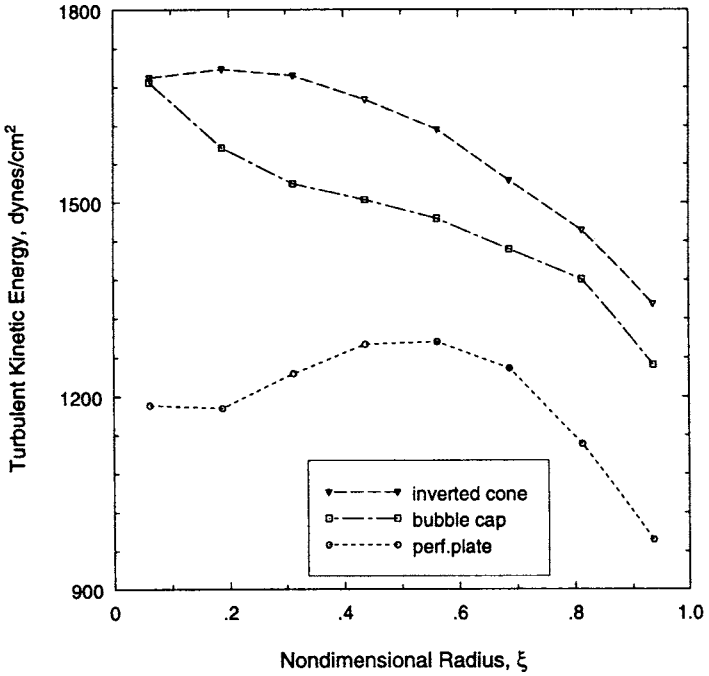

Figure 1.2 Effect of the Distributor on Turbulent Kinetic Energy in a 19-cm Diameter Column, *U*g = 12.0 cm/s. Distributors are cone (8C): one point inlet (1.27 cm in diameter); bubble cap (8B); perforated plate (8A): 0.33 mm hole diameter and 0.05% open area.

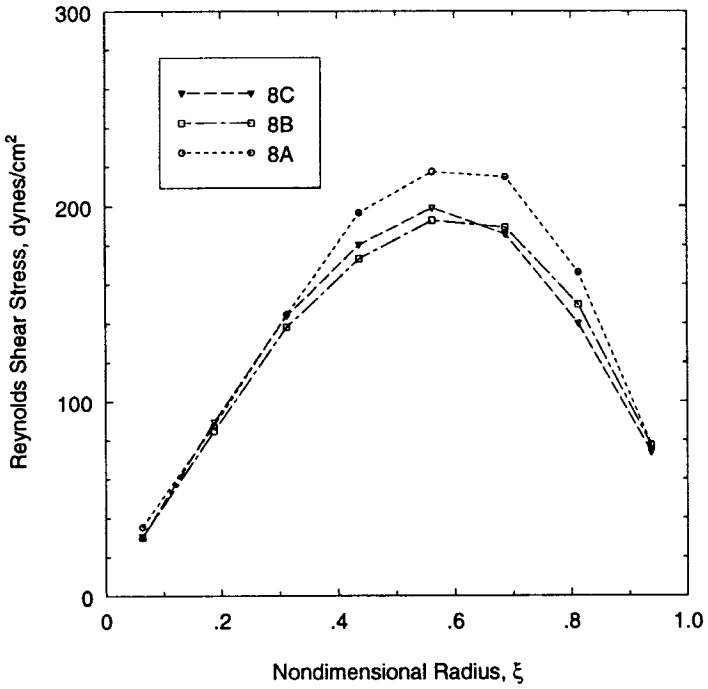

Figure 1.3 Effect of Distributor on Reynolds Shear Stress in a 19-cm Diameter Column, *U*g = 12.0 cm/s. Distributors are cone (8C): one point inlet (1.27 cm in diameter); bubble cap (8B); perforated plate (8A): 0.33 mm hole diameter and 0.05% open area.

2. SIMULATION OF GAS-LIQUID FLOW IN CYLINDRICAL BUBBLE COLUMNS WITH FLUENT: COMPARISON WITH CARPT-CT EXPERIMENTS RESULTS

2.1 Motivation

Validation of a transient, two-dimensional (2D), axisymmetric simulation of a laboratory-scale cylindrical bubble column was attempted against the experimental data collected using the CARPT and CT techniques in our laboratory under operating conditions identical to those used with simulation. The numerical simulation was effected using the FLUENT library of codes. The present work uses a 2D CFD model as a computational simplification for simulating the three-dimensional (3D) flow in order to evaluate which experimental features can be captured by this simplified model.

From our earlier work on computational fluid dynamic simulations of bubble columns using the CFDLIB codes from Los Alamos National Laboratory, we had concluded that it is necessary to perform fully 3D simulations for capturing the transient flow profiles in 3D, cylindrical bubble columns. However, 2D, axisymmetric simulations can serve as an engineering simplification that is computationally significantly less demanding than the 3D version. Using CFDLIB framework, we have shown that time-averaged liquid velocity profiles can be predicted well, but that gas holdup profiles are not captured with fidelity.

Using FLUENT, which has numerical schemes that are distinctly different from CFDLIB and which also employs a wider variety of closure schemes, we intended to test how far one can progress with the 2D version for bubble column simulations. In the process, we familiarized ourselves with the details of the package, and initiated a systematic study to investigate the capabilities and features of the code for simulating 3D, two-phase flows in bubble columns. In the near future, these 2D routines (of FLUENT) will also be tested against the experiments done in 2D bubble columns by our collaborators at Ohio State University. This series of investigations should build a solid framework for 3D simulations in the future, coupled with heat transfer, mass transfer, volatility effects and chemical reactions.

2.2 Results and Discussion

Two-Fluid Euler-Euler Model:

In the Eulerian two-fluid approach (Anderson and Jackson, 1967), the two phases (gas and liquid) are treated as interpenetrating continua, and the probability of occurrence of any one phase in multiple realizations of the flow is given by the instantaneous volume fraction of that phase at that point. The sum total of all volume fractions at a point is identically unity. Both fluids are treated as incompressible, and a single pressure field is shared by all phases. Continuity and momentum equations are solved for each phase. Momentum transfer between the phases is modeled through a drag term, which is a function of the local slip velocity between the phases. A characteristic diameter is assigned to the dispersed phase gas bubbles, and a drag

formulation based on a single sphere settling in an infinite medium is used (Morsi and Alexander, 1972). Turbulence in either phase is modeled separately using the standard k-ε model, modified with terms accounting for two-phase flow (Elghobashi and Abou-Arab, 1983).

Algebraic Slip Mixture Model (ASMM):

The ASMM (Manninen *et al.,* 1996) also models the phases as two interpenetrating continua, with the probability of existence of each phase at a point in the computational domain given by its respective volume fraction (holdup). In general, the two phases move at different velocities. However, in contrast to the two-fluid Euler-Euler approach, a *single* equation is solved each for the continuity and for the momentum of the *mixture*. The motion of each phase relative to the center of mass of the mixture in any control volume is viewed as a diffusion of that phase; this introduces the concept of a diffusion velocity of each phase (which is analogous and directly related to the slip velocity and the drift velocity, as referred to in the classical drift flux model for a mixture (Wallis, 1969)). Since the equations are solved for the mixture, no formulation for *drag* (which models momentum transfer *between* the phases) is required.

The Reynolds averaged mixture momentum equation has a term, called the *diffusion stress*, which results from the relative slip between the two phases. This requires closure in terms of the diffusion velocity of each phase (or, equivalently, the drift or the slip velocity between the phases). In the ASMM, this requirement is supplied by assuming that the phases are in *local equilibrium* over *short spatial length scales*. This means that the dispersed phase entity (bubble, particle) always slips with respect to the continuous phase at its terminal Stokes velocity in the local acceleration field.

The *diffusion stress* term is also the only term in which the phase volume fractions appear explicitly. In order to back out the individual phase velocities and volume fraction at the end of the computation at each time step, it is necessary to solve a differential equation for volume fraction of the dispersed phase, coupled with the solution of the mixture equations. This equation is obtained from the equation of continuity for the dispersed phase. Finally, the turbulent stress term in the mixture equation is closed by solving a k-ε model for the *mixture* phase.

A detailed description and the equations used for either model are discussed in the topical report that will follow.

Simulation Predictions:

Figure 2.1 presents a liquid time-averaged velocity vector plot of the simulated flow profile, using the Euler-Euler two-fluid model at the gas superficial velocities of 2 cm s^{-1} and 12 cm s^{-1} (the vector plots are "mirrored" about the axis of symmetry). Similar results are also seen with the ASMM simulations. The time-averaged simulation profiles (axisymmetric) are qualitatively similar to the experimental flow profiles observed from the CARPT experiments (Degaleesan, 1997). One observes a single circulation loop, with the liquid ascending at the center of the

column and descending at the walls. Naturally, no asymmetries are observed at the distributor because the gas in the simulation is introduced through a uniform plate, and a real sparger has not been modeled.

In Figure 2.2 the time-averaged liquid axial velocity profiles are compared against the time-averaged velocity profiles obtained by CARPT. Figure 2.3 shows the comparison for gas holdup profiles obtained from the simulations and from Computed Tomography (CT). Results presented are at a height of 53 cm above the distributor, typical of the fully developed region of the flow. All the simulations showed that there is no significant axial variation in any of the variables in the zone of developed flow. The centerline axial velocity is over-predicted by both the Euler-Euler two-fluid model, as well as by the ASMM. However, the general shape of the profile is well captured, and the discrepancy in the model predicted and the CARPT-measured, time-averaged axial liquid velocity diminishes as one moves radially outwards in the column. It is also possible to predict reasonably well the *velocity inversion point* (i.e., the radial location where the axial velocity component becomes zero).

Figure 2.3 shows that in the bubbly flow regime (U_g = 2 cm s^{-1}), both the ASMM and the two-fluid models seem to predict the mean holdup profile well. In the churn-turbulent regime, however, there is still a discrepancy between predictions and data, although the roughly parabolic profile observed in practice is seen in the simulation results as well. The higher volume fraction of gas at the center of the column drives the liquid flow upwards at a high velocity due to gas buoyancy, and the liquid, which is in batch mode, returns downwards at the periphery.

A comparison of kinetic energy profiles obtained by solution of the k-ε model in the simulations and those measured via CARPT also showed good agreement (Figure 2.4). Kinetic energy profiles typically exhibit a maximum around the *velocity inversion point*, due to large gradients and large fluctuations in the liquid velocity. In the bubbly regime, this effect is not very significant (because of suppressed turbulence), and the turbulent kinetic energy is practically flat as a function of radius. These effects are clearly captured in the simulation results presented in Figure 2.4. (It may be noted that for the ASMM, the kinetic energy plotted in Figure 2.4 is the *mixture* kinetic energy in contrast to the liquid phase turbulent kinetic energy. However, it can be readily shown that due to the significantly lower gas phase density, liquid phase inertia predominates and is the dominant contributor to the mixture kinetic energy.)

A detailed discussion of results, the numerical approach and the models employed, as well as a comparison with full 3D simulations, will be presented in future quarterly and topical reports.

2.3 References:

Anderson, T. B. and Jackson, R. (1967) A Fluid Dynamical Description of Fluidized Beds. *Ind. Engng. Chem. Fund.* 6, 527-534.

Degaleesan, S. (1997) Fluid Dynamic Measurements and Modeling of Liquid Mixing in Bubble Columns. *D. Sc. Thesis*, Washington University in St. Louis, Missouri, USA.

Elgobashi, S. E. and Abou-Arab, T. W. (1983) A Two-Equation Turbulence Model for Two-Phase Flows. *Phys. Fluids* 26(4), 931-938.

Morsi, S. A. and Alexander, A. J. (1972) An Investigation of Particle Trajectories in Two-Phase Flow Systems. *J. Fluid Mech.* 55(2), 193-208.

Manninen, M., Taivassalo, V. and Kallio, S. (1996) *On the Mixture Model for Multiphase Flow*, VIT Publications, Technical Research Center of Finland.

Wallis, G. (1969) *One-Dimensional Two-Phase Flow*, McGraw-Hill, New York, USA.

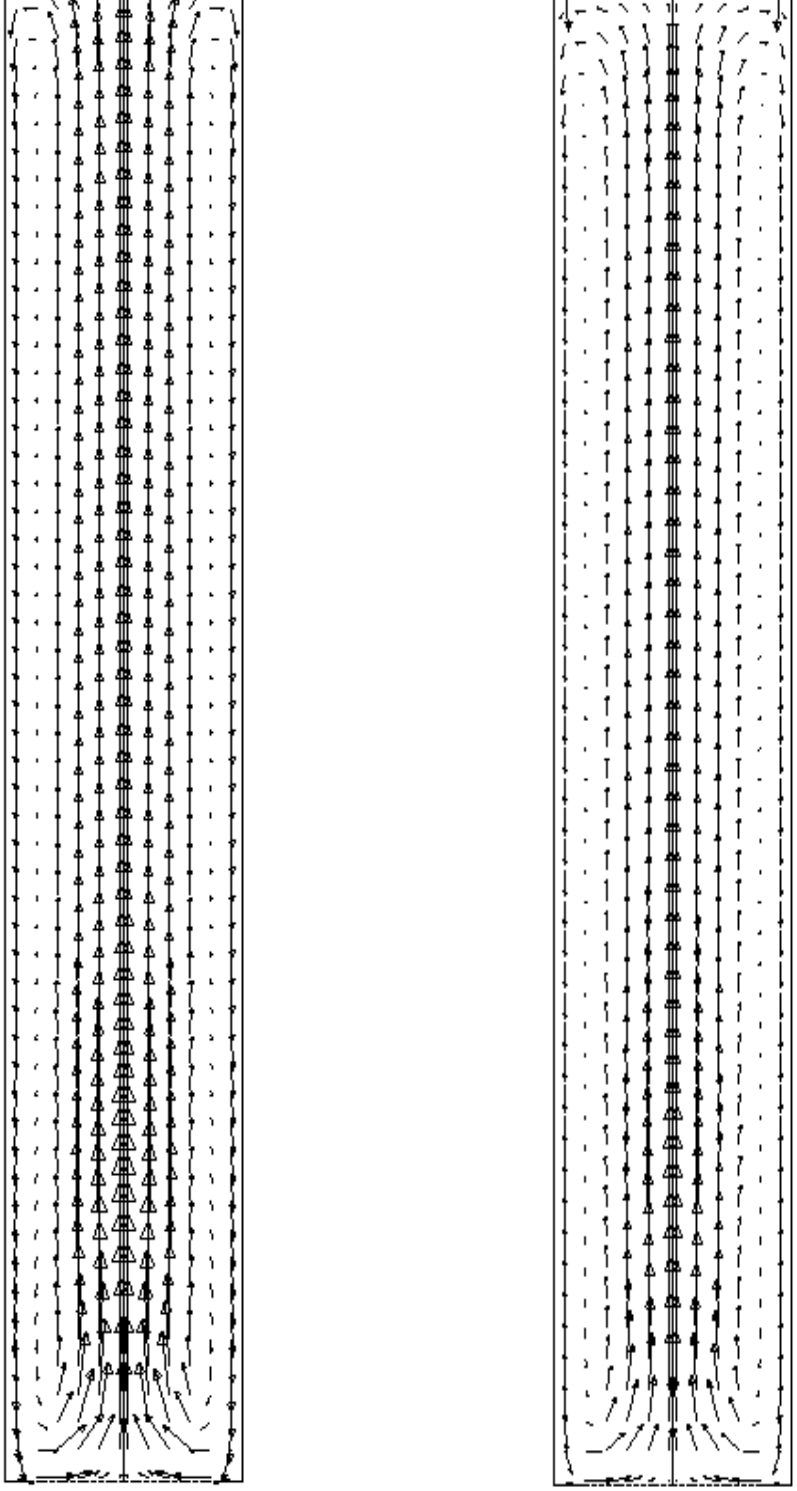

(a) (b)

Figure 2.1 Velocity Vector Plots obtained from Simulations: (a) U_g = 2.0 cm/s (Two Fluid) (b) U_g = 12.0 cm/s (Two Fluid). (The r-z plane has been "mirrored" along the axis of symmetry to show the vector field across the diameter.)

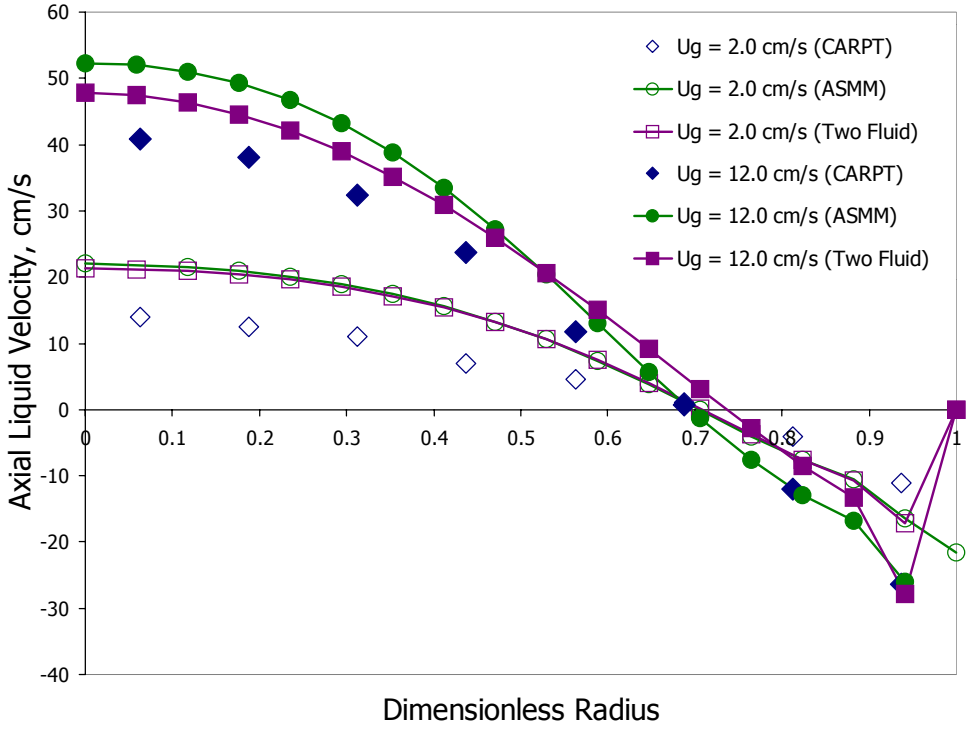

Figure 2.2 Comparison of Axial Liquid Velocity Profiles

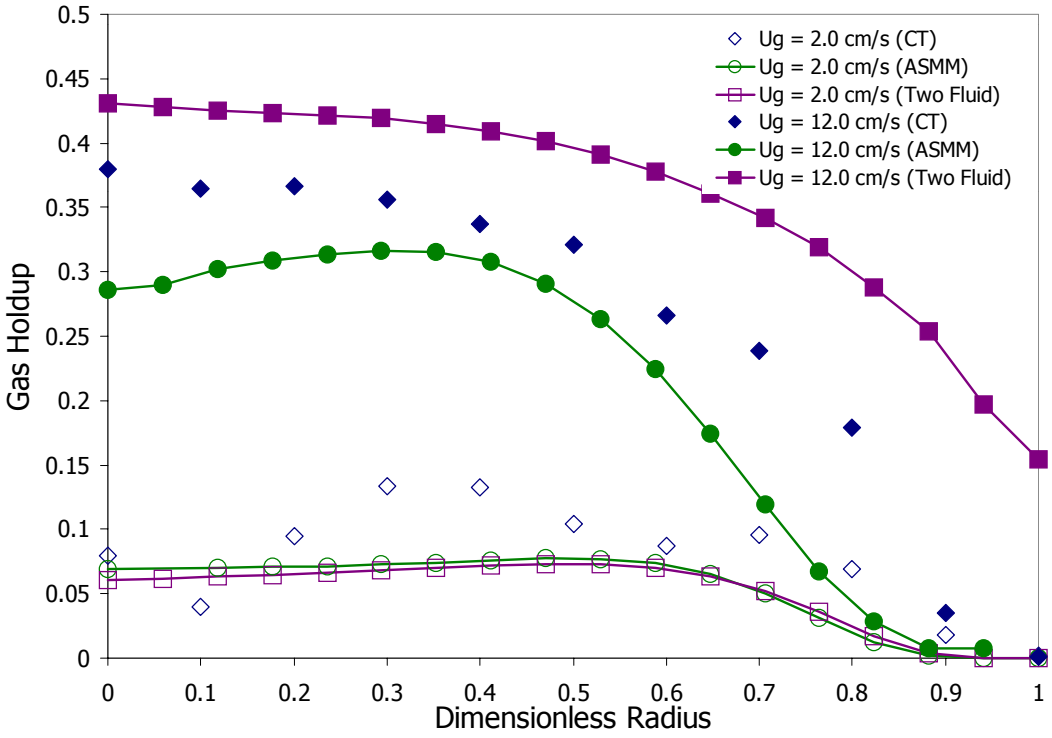

Figure 2.3 Comparison of Gas Holdup Profiles

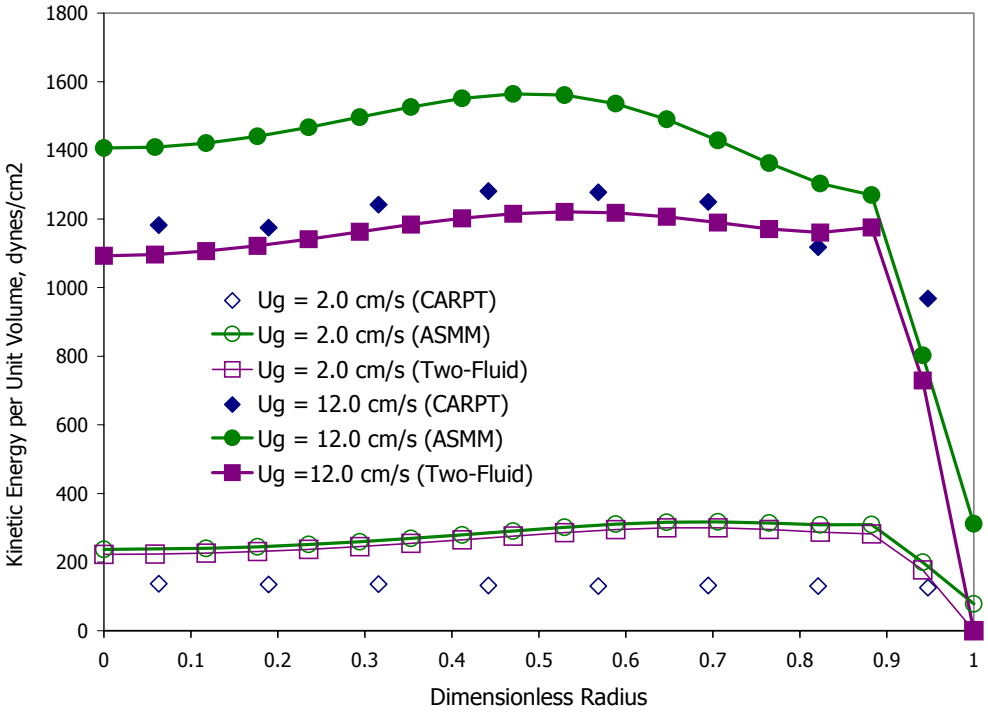

Figure 2.4 Comparison of Turbulent Kinetic Energy Profiles

The Ohio State University Research

The report from the Ohio State University for the period follows.

INTRINSIC FLOW BEHAVIOR IN A SLURRY BUBBLE COLUMN UNDER HIGH PRESSURE AND HIGH TEMPERATURE CONDITIONS

Quarter Report

(**Reporting Period:** October 1 to December 31, 1998)

Highlights

- A mechanistic model was developed to predict the initial bubble size in liquid-solids suspensions under high-pressure conditions. This was accomplished by taking into account the resistance to the bubble growth induced by the presence of the particles, i.e., suspension inertial force and particle-bubble collision force.

- It was found that the dominant forces in the bubble formation process are buoyancy and suspension inertial forces. An analytical expression was proposed to evaluate the suspension inertial force based on the flow field of the suspension around a growing bubble. The flow field around the bubble was measured using a high-speed particle image velocimetry (PIV) technique.

- The model can reasonably predict the initial bubble size measured in this study and reported in the literature. Based on this model, the effects of solids concentration and pressure on the bubble formation process were analyzed. When the solids concentration increased, the suspension inertial force increased, leading to an increased initial bubble size.

- Under constant flow conditions, the effect of pressure on initial bubble size was insignificant in the liquid-solid suspension, as well as in the liquid. The model could predict the negligible pressure effect.

- Bubble size variation is important for understanding the pressure effect on hydrodynamics. The upper limit of the bubble size is set by the maximum stable bubble size. A mechanistic model based on the concept of internal gas circulation inside a bubble was proposed to simulate the maximum stable bubble size in a high-pressure slurry bubble column.

Work Performed

PIV Experimental Setup

The suspension inertial force, $F_{I,m}$, which is essentially the rate of momentum change of the liquid and particles with respect to time, based on Newton's second law, is:

$$F_{I,m} = \frac{\mathrm{d}\left[\iiint\left(\varepsilon_s \rho_s u_s + \varepsilon_l \rho_l u_l\right)\delta V\right]}{\mathrm{d}t} \approx \frac{\mathrm{d}\left(\iiint \rho_m u_m \delta V\right)}{\mathrm{d}t} \qquad (1)$$

To evaluate the inertial force of the liquid-solid suspension based on Eq. (1), the flow field of the liquid-solid suspension around a growing bubble from an injector must be known. The flow field was measured in a two-dimensional (2D) liquid-solid suspension with a high-speed particle image velocimetry (PIV) technique. Figure 1 shows the experimental apparatus. The 2D fluidized bed is made of Plexiglas, and the viewing section of the column is 30 cm in width, 130 cm in height and 0.6 cm in depth. Below the viewing section is the liquid distributor, which consists of a packed particle section and a liquid calming section. Compressed air and glycerin solutions are used as the gas and liquid phases. The gas is injected by a tube flush mounted on the column wall. The gas injector opening is 1.6 mm ID. A manual solenoid valve, creating single bubbles of various sizes, regulates the gas flow through the injector.

Activated carbon particles with a size range from 500 to 800 μm are used as the solid phase. Approximately 2% of the particles are colored white and are utilized as the tracers. The CCD image recorded by the high-speed camera features 765 pixels across by 246 lines. The framing rate of the camera can be selected up to 480 fields/sec. A frame grabber, which is equipped with 40 MHz max pixel clock to support the high-framing rate, simultaneously digitizes the CCD image from the camera. Further, the high-speed camera is connected to the high-speed video recorder to store the images for further studies. The PIV technique used here employs a particle-tracking algorithm developed by Chen and Fan (1992) to determine the velocity fields of the particles. The particle-tracking algorithm involves matching of the particles in three or more consecutive fields. The PIV system provides data on the full-field velocities of the tracer particles.

Suspension Inertial Force

Acceleration of the liquid-solid mixture associated with the bubble induces significant resistance to the motion of the bubble. The suspension inertial force can be evaluated by considering the flow field of the mixture around the bubble, as described by Eq. (1). Figure 2 shows the particle velocity field obtained from the PIV analysis. Since the particle terminal velocity in the liquid is small, the particle velocity can be used to approximate the flow field of the liquid-solid suspension. It can be seen from Figure 2 that the particles on the bubble surface have the same velocity as the bubble. As the distance of the particle from the bubble surface increases, the particle velocity decreases. The particle velocity field shown in the figure can be approximated

by

$$u_m = u_b \exp\left[k\left(\frac{r}{r_b}-1\right)\right] \tag{2}$$

where k = -0.64. For a 2D flow field, the suspension inertial force is evaluated by

$$F_{I,m} = \frac{\mathrm{d}\iint \rho_m u_m \delta A}{\mathrm{d}t} \tag{3}$$

Integration of Eq. (3) from r_0 to R where $u_m = 0.01u_b$ gives

$$\begin{aligned} F_{I,m} = \frac{d\left(\iint \rho_m u_m \delta A\right)}{\mathrm{d}t} &= \frac{\mathrm{d}}{\mathrm{d}t}\int_0^{\pi}\mathrm{d}\theta \int_{r_b}^{R} \rho_m u_b \exp\left[k\left(\frac{r}{r_b}-1\right)\right] r\mathrm{d}r \\ &= \left\{ \frac{\left(\frac{kr}{r_b}-1\right)\exp\left[k\left(\frac{r}{r_b}-1\right)\right]}{k^2} \frac{\mathrm{d}}{\mathrm{d}t}\left[\rho_m\left(\pi r_b^2\right)u_b\right] \right\}\Bigg|_{r_b}^{R} \\ &= 3.86\frac{\mathrm{d}}{\mathrm{d}t}\left[\rho_m\left(\pi r_b^2\right)u_b\right] \end{aligned} \tag{4}$$

Equation (4) indicates that the suspension inertial force is equivalent to 3.86 times the change rate of the momentum of the suspension that is displaced by the bubble. Assume that the suspension inertial force from the 2D measurement can be extended to describe the suspension inertial force under 3D conditions, i.e.,

$$F_{I,m} = \iiint \rho_m u_m \delta V = 3.86\frac{\mathrm{d}}{\mathrm{d}t}\left[\rho_m\left(\frac{1}{6}\pi d_b^3\right)u_b\right] \tag{5}$$

In principle, the coefficient (3.86) in Eq. (5) is a function of solids holdup, particle properties, and liquid properties. In this study, the value of 3.86 is used for the coefficient as an approximation in predicting the initial bubble size in liquid-solid suspensions. When the solids holdup is zero or the particle density is equal to the liquid density, the coefficient would assume a value of 11/16, the value that characterizes the added mass effects for liquid (Davidson and Schuler, 1961; Ramakrishnan et al., 1969).

Simulation Results of Initial Bubble Size

Particle Effects

Figure 3 shows the particle effect on initial bubble size. Various solids holdups in the suspension are obtained by varying the fluidizing liquid velocity. The fluidizing liquid velocity is so small that it does not affect bubble formation behavior. At both the ambient and 4.2 MPa pressures, the bubbles formed in the liquid-solid suspension are larger than those formed in the liquid for a given orifice gas velocity. The bubble size increases with an increase in solids holdup. Figure 3 shows that the model developed in this work can reasonably predict the initial bubble size in the liquid-solid suspensions under various pressure conditions. The experimental data of Massimilla et al. (1961) showed a similar trend. The above results apparently contradict the conclusions drawn by Yoo et al. (1997), who indicated that particles do not have a significant effect on the initial bubble size in their experimental system. As shown in Figure 4, the model proposed in this study can also reasonably predict the experimental data under constant flow conditions reported by Yoo et al. (1997). Thus, the effect of particles on the initial bubble size depends on the physical properties of the liquid and solids phases employed.

The initial bubble size is determined based on the balance of various forces acting on the bubble formed at the nozzle. In liquids, the upward forces (driving forces) include buoyancy and gas momentum forces, and the downward forces (resistances) include liquid drag, surface tension, gas bubble inertial force, and Basset force. The presence of particles induces two additional downward forces on the bubble: particle-bubble collision force and liquid-solid suspension inertial force. Based on expressions of these two forces as presented in the previous reports, both the collision and suspension inertial forces increase linearly with solids holdup. Figure 5 compares the magnitude of all the forces involved in the bubble formation process. Among the resistances, the suspension inertial force is dominant, while buoyancy is dominant as a driving force compared to the gas momentum force. With a much smaller inertial force for the liquid compared to the liquid-solid suspension, the bubble center accelerates and moves faster in the former than in the latter under the same pressure, temperature, and gas flow-rate conditions; hence, the bubble detaches from the nozzle at an earlier time in the liquid. Therefore, the initial bubble size in the liquid is much smaller than that in the liquid-solid suspension. When the solids holdup increases, the suspension inertial force increases, leading to an increased initial bubble size.

Pressure Effect

The experimental data shown in Figure 6 indicate that the effect of pressure on the initial bubble size is insignificant in the liquid-solid suspension, as well as in the liquid under the conditions of this study. Increasing pressure does not significantly change the bubble sizes for a given solids holdup, orifice gas velocity, and temperature. The model's prediction is consistent with the experimental results obtained in this study, as shown in Figure 6. As discussed in the preceding section, the initial bubble size is determined based on the balance among various forces acting on the bubbles. The magnitudes of all the forces are pressure dependent (Figure 7). When the pressure increases, the gas momentum increases significantly. However, the effect of the increase in gas momentum force is counterbalanced by the decrease in the buoyancy force and

the increases in the Basset and liquid drag forces. Under the constant flow conditions, the effects of pressure on the overall upward forces and overall downward forces are comparable, leading to an insignificant net effect of pressure on the initial bubble size in liquid-solid suspensions. This mechanism can also explain the negligible pressure effect on bubble formation under constant flow conditions, as indicated by the results of Wilkinson and Van Dierendonck (1994) and Yoo et al. (1997).

Maximum Stable Bubble Size

Introduction

Bubble size variation with pressure is key to understanding pressure effects on hydrodynamics. The upper limit of the bubble size is set by the maximum stable bubble size, D_{max}, above which the bubble is subjected to breakup and is hence unstable. Several mechanisms have been proposed to predict the maximum stable bubble size in gas-liquid systems. Hinze et al. (1955) proposed that bubble breakup is caused by the dynamic pressure and the shear stresses on the bubble surface induced by different liquid flow patterns, e.g., shear flow and turbulence. When the maximum hydrodynamic force in the liquid is larger than the surface tension force, the bubble disintegrates into smaller bubbles. This mechanism can be quantified by the liquid Weber number; when the Weber number, which equals $\rho_l \overline{u^2} D_{max} / \sigma$, is larger than a critical value, the bubble is not stable and disintegrates. This theory was adopted to predict the breakup of bubbles in gas-liquid systems (Walter and Blanch, 1986). Calculations by Lin et al. (1998) showed that the theory under-predicts the maximum bubble size and cannot predict the observed effect of pressure on bubble size.

A maximum stable bubble size exists for bubbles rising freely in a stagnant liquid without the external stresses (Grace et al., 1978). Rayleigh-Taylor instability has been regarded as the mechanism for the bubble breakup under such conditions. A horizontal interface between two stationary fluids is unstable with respect to disturbances having wavelengths exceeding a critical value if the upper fluid has a higher density than the lower one (Bellman and Pennington, 1954). Chen and Fan (1988) obtained an expression for the critical wavelength for a curved surface as in the case of bubbles. Grace et al. (1978) applied the Rayleigh-Taylor instability theory by considering the time available for the disturbance to grow and the time required for the disturbance to grow to an adequate amplitude. Batchelor (1987) pointed out that the observed maximum air bubbles in water are considerably larger than those predicted by the model of Grace et al. (1978). Batchelor (1987) further took into account the stabilizing effects of liquid acceleration along the bubble surface and the non-constant growth rate of the disturbance. In his model, the information on disturbances is required to predict the maximum bubble size. The models based on the Rayleigh-Taylor instability predict an almost negligible pressure effect on the maximum bubble size; in fact, the Rayleigh-Taylor instability implies that the bubble is slightly more stable when the gas density is higher.

Kitscha and Kocamustafaogullari (1989) applied the Kelvin-Helmhotz instability theory to model the breakup of large bubbles in liquids, using the same concept of Grace et al. (1978). Wilkinson and Van Dierendonck (1990) applied the critical wavelength to explain the maximum

stable bubble size in high-pressure bubble columns. Their results showed that the critical wavelength decreases with an increase in pressure, and therefore bubbles are easier to disintegrate by the disturbances. However, the critical wavelength is not necessarily equivalent to the maximum stable bubble size, and their approach alone cannot quantify the pressure effect on bubble size.

All the models mentioned above ignored the effect of internal circulation of the gas. For the continuity of the tangential velocity in the gas and liquid phases, the internal circulation velocity is of the same order of magnitude as the bubble rise velocity. A centrifugal force is induced by this circulation, pointing outwards to the bubble surface, which can suppress the disturbances at the gas-liquid interface and act as a stabilizing force. This force may also explain the underestimation of D_{max} by the model of Grace et al. (1978), besides that discussed by Batchelor (1987). On the other hand, centrifugal force can also disintegrate the bubble as the force increases with an increase in bubble size. The bubble breaks up when the centrifugal force exceeds the surface tension force, especially at high pressures when gas density is high.

Levich (1962) recognized the fact of internal gas circulation and assumed the centrifugal force to be equal to the dynamic pressure induced by the gas moving at the bubble rise velocity, and proposed a simple equation to calculate the maximum stable bubble size:

$$D_{\max} \approx \frac{3.63\sigma}{u_b^2 \sqrt[3]{\rho_l^2 \rho_g}} \tag{6}$$

Equation (6) shows a significant effect of pressure on the maximum bubble size; however, it severely under-predicts the maximum bubble size.

In this work, the mechanism for bubble breakup is illustrated by a concept of internal gas circulation inside a bubble, and an analytical expression is obtained to predict the maximum stable bubble size over the wide pressure range. The details of this model will be presented in the next monthly reports.

Notations

A	Cross-sectional area
D_0	Orifice diameter
$D_{\max}$	Maximum stable bubble size
$F_{I,m}$	Suspension inertial force
k	Constant in Eq.(2)
Q	Volumetric gas flow rate
r	Radial position
r_b	Bubble radius
t	Time
u_0	Orifice gas velocity

u_b Bubble rise velocity
u_b Rise velocity of bubble center
u_l Liquid velocity
u_m Velocity of suspension
u_s Particle velocity
$\overline{u^2}$ Average value of the squares of velocity differences over a distance of D_{max} across the whole flow field

Greek letters
ε Phase holdup
ρ Density
σ Gas-liquid surface tension

Subscripts
g Gas phase
l Liquid phase
m Suspension
s Solid phase

References

Batchelor, G.K., "The Stability of a Large Gas Bubble Rising through Liquid," *J. Fluid Mech.*, **184**, 399 (1987).

Bellman, R. and R.H. Pennington, "Effect of Surface Tension and Viscosity on Taylor Instability," *Q. Appl. Math*., **51**, 151 (1954).

Chen, R. C. and L.-S. Fan, "Particle image velocimetry for characterizing the flow structure in three-dimensional gas-liquid-solid fluidized beds," *Chem. Eng. Sci*., **47**, 3615 (1992).

Chen, Y.-M. and L.-S. Fan, "On the Criteria of Rayleigh-Taylor Instability at a Curved Interface by a Local Force Balance," unpublished results (1988).

Davidson, J. F. and B. O. G. Schuler, "Bubble formation at an orifice in an inviscid liquid," *Trans. Instn. Chem. Engrs*., **38**, 335 (1961).

Grace, J.R., T. Wairegi, and J. Brophy, "Break-Up of Drops and Bubbles in Stagnant Media," *Can. J. Chem. Eng*., **56**, 3 (1978).

Hinze, J.O., "Fundamentals of the Hydrodynamic Mechanism of Splitting in Dispersion Processes," *AIChE J*., **1**, 289 (1955).

Kitscha, J. and G. Kocamustafaogullari, "Breakup Criteria for Fluid Particles," *Int. J. Multiphase Flow*, **15**, 573 (1989).

Levich, V.G., *Physiochemical Hydrodynamics*, Prentice Hall, Englewood Cliffs, NJ (1962).

Lin, T.-J., K. Tsuchiya, and L.-S. Fan, "Bubble Flow Characteristics in Bubble Columns at Elevated Pressure and Temperature," *AIChE J*., **44**, 545 (1998).

Massimilla, L., A. Solimando and E. Squillace, "Gas dispersion in solid-liquid fluidized beds," *Brit. Chem. Eng.*, **6**, 232 (1961).

Ramakrishnan, S., R. Kumar and N. R. Kuloor, "Studies in bubble formation – I: bubble formation under constant flow conditions," *Chem. Eng. Sci*., **24**, 731 (1969).

Walter, J.F., and H.W. Blanch, "Bubble Break-Up in Gas-Liquid Bioreactors: Break-Up in

Turbulent Flows," *Chem. Eng. J*., **32**, B7 (1986).
Wilkinson, P. and L.L. van Dierendonck, "Pressure and Gas Density Effects on Bubble Break-Up and Gas Holdup in Bubble Columns," *Chem. Eng. Sci*., **8**, 2309 (1990).
Wilkinson, P. M. and L. Van Dierendonck, "A theoretical model for the influence of gas properties and pressure on single-bubble formation at an orifice," *Chem. Eng. Sci*., **49**, 1429 (1994).
Yoo, D.-H., H. Tsuge, K. Terasaka and K. Mizutani, "Behavior of bubble formation in suspended solution for an elevated pressure system," *Chem. Eng. Sci*., **52**, 3701 (1997).

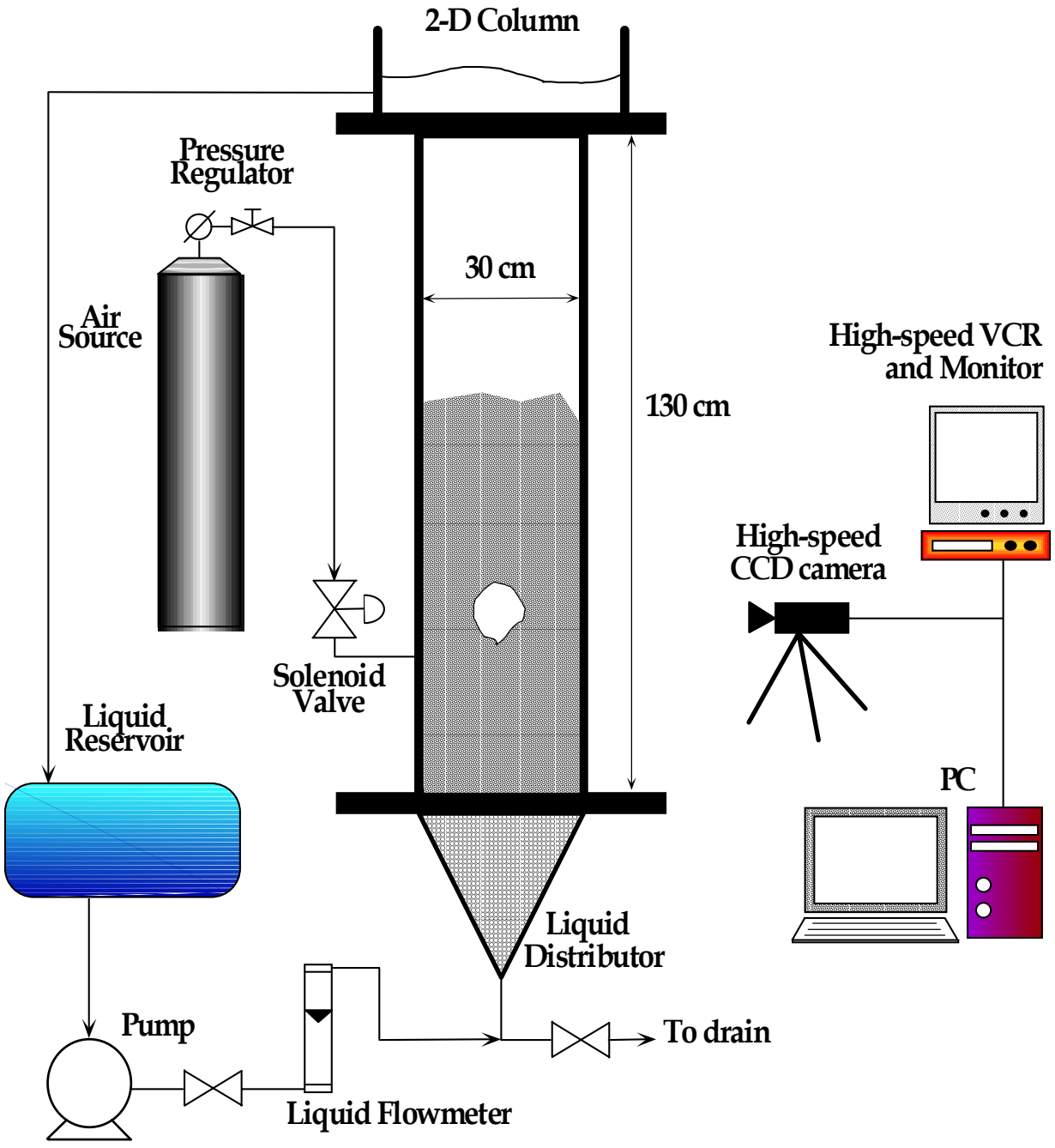

Figure 1 Experimental Setup for Measurement of the Flow Field Around a Growing Bubble in Liquid-Solid Suspensions

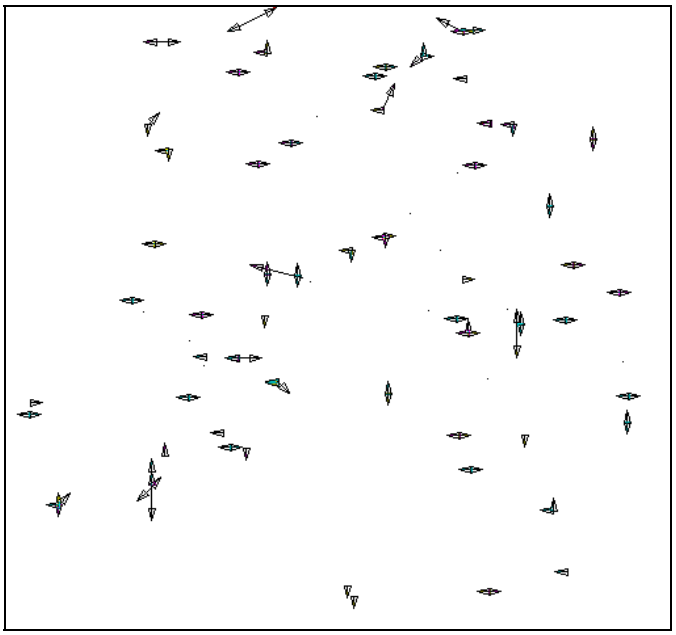

(a)

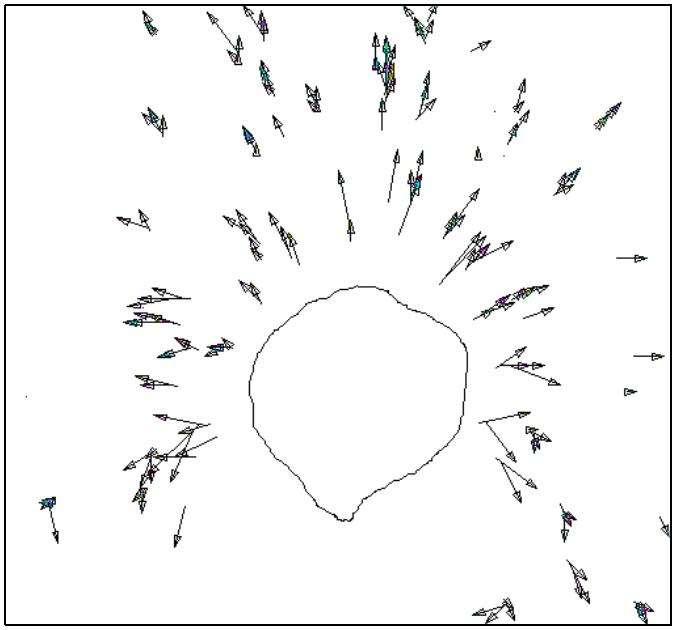

(b)

Figure 2 (a) Particle Velocities Before Bubble Injection; (b) Particle Velocities Around a Growing Bubble

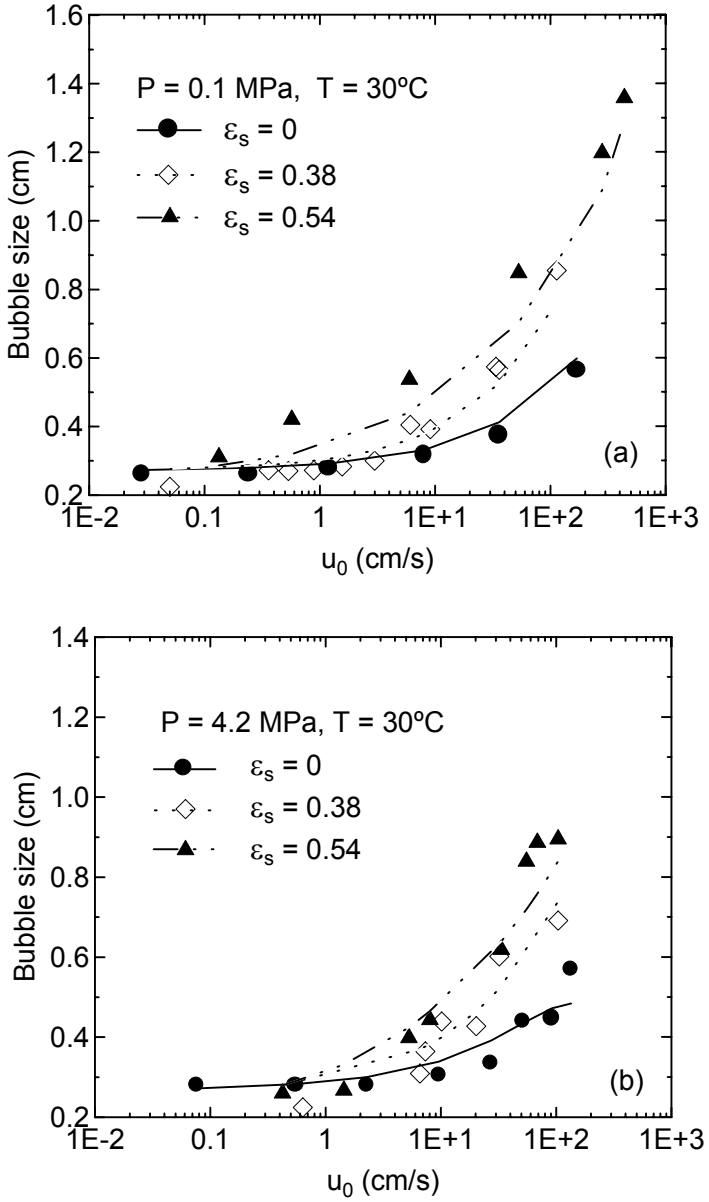

Figure 3 Effect of Solids Holdup on Initial Bubble Size (a) Pressure = 0.1 MPa; (b) Pressure = 4.2 MPa (symbols: experimental data; lines: model predictions)

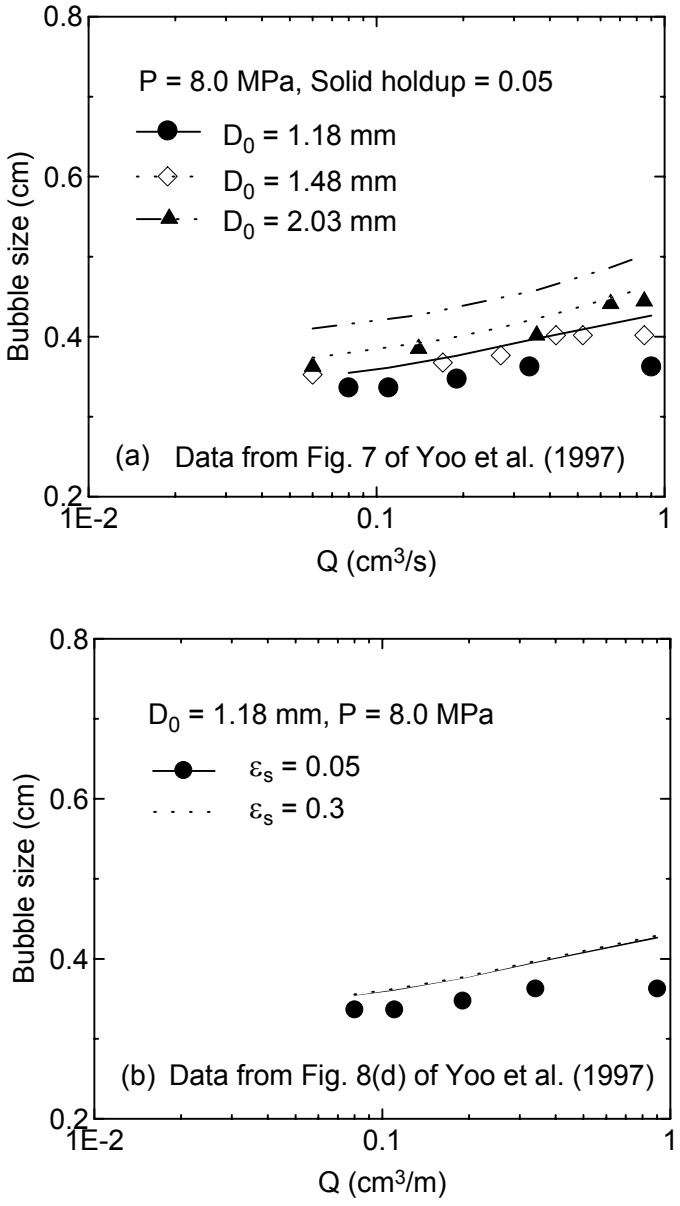

Figure 4 Comparison Between the Experimental Data of Yoo et al. (1997) and the Predictions by the Present Model (symbols: experimental data; lines: model predictions)

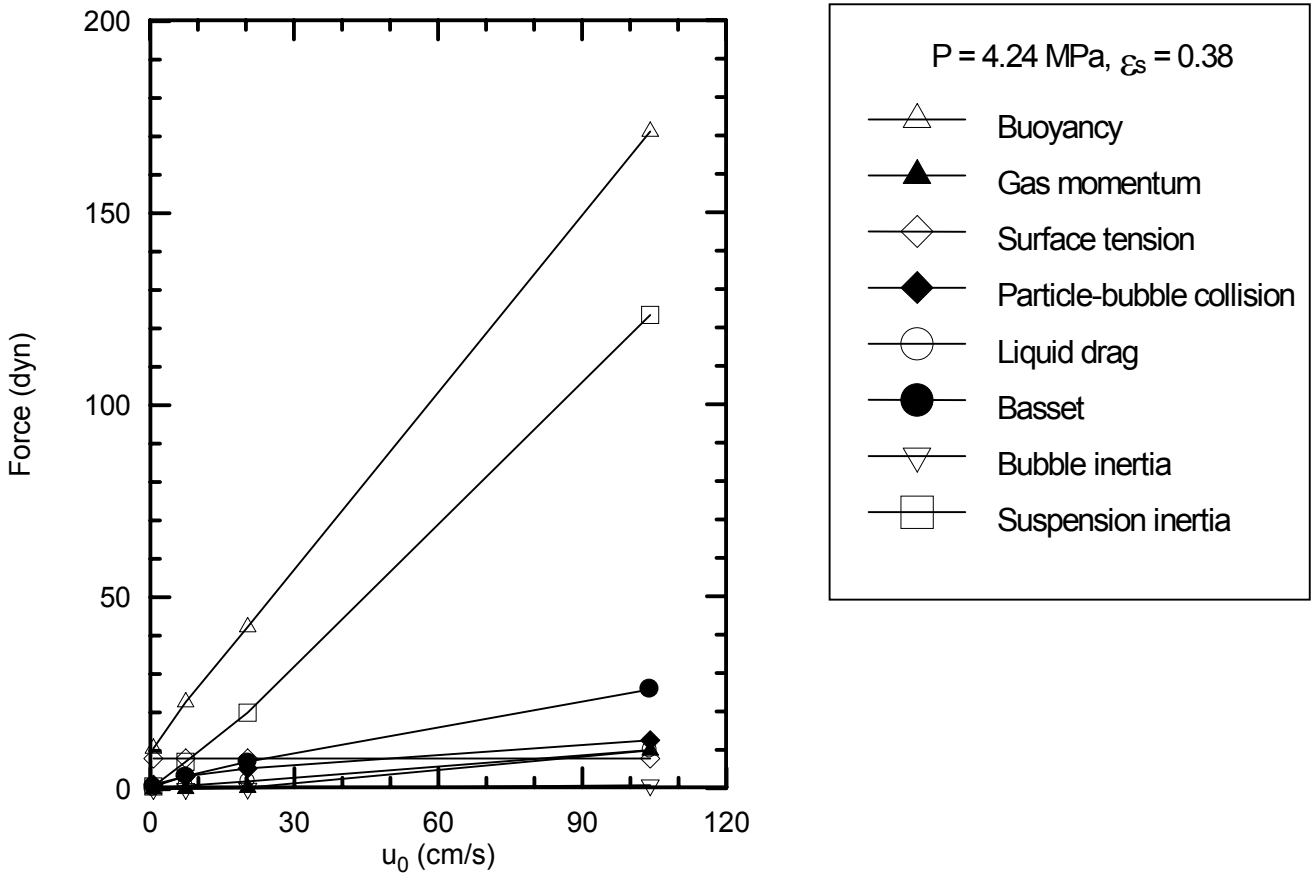

Figure 5 Comparison of Various Forces Acting on the Growing Bubble in the Bubble Formation Process

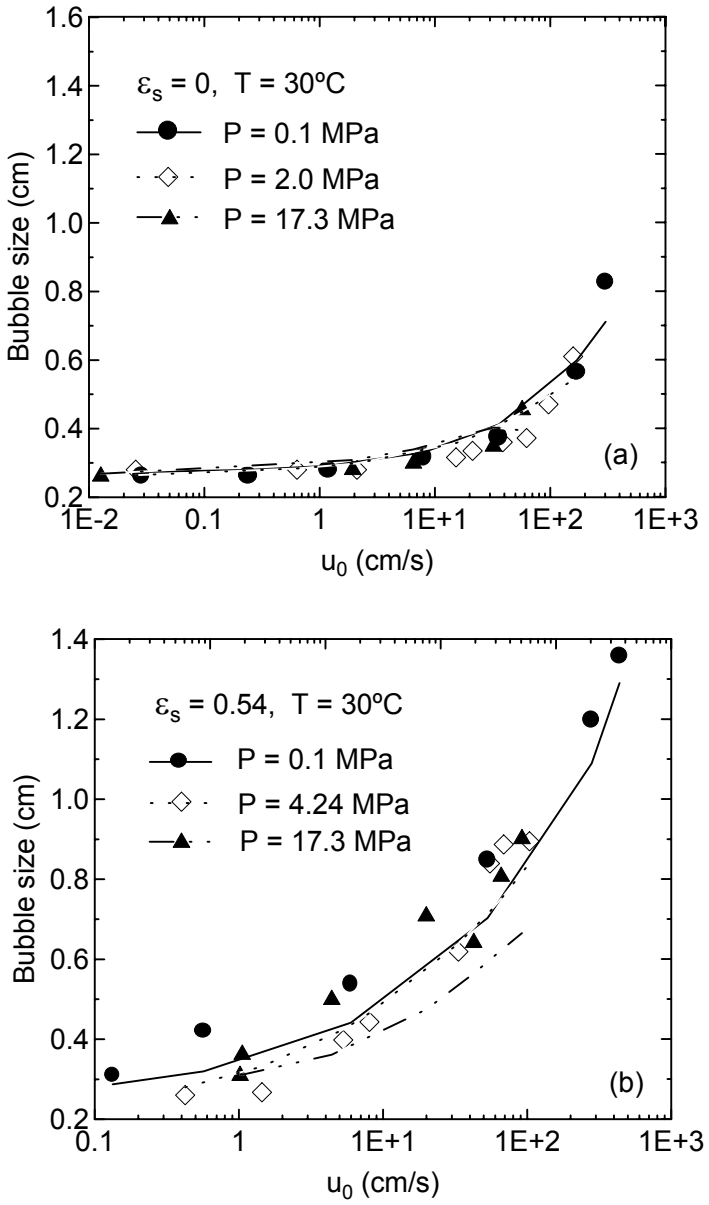

Figure 6 Effect of Pressure on Initial Bubble Size in Liquid and in Liquid-Solid Suspensions (symbols: experimental data; lines: model predictions)

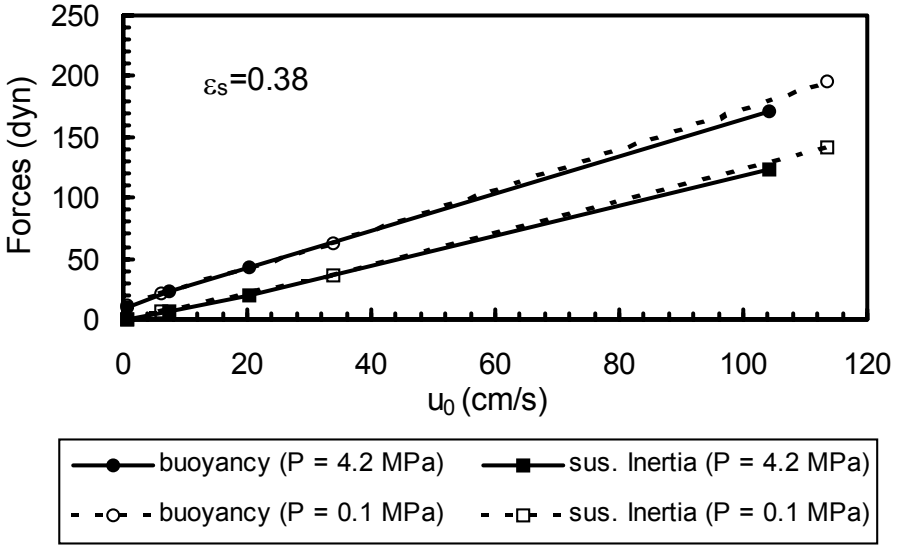

(a)

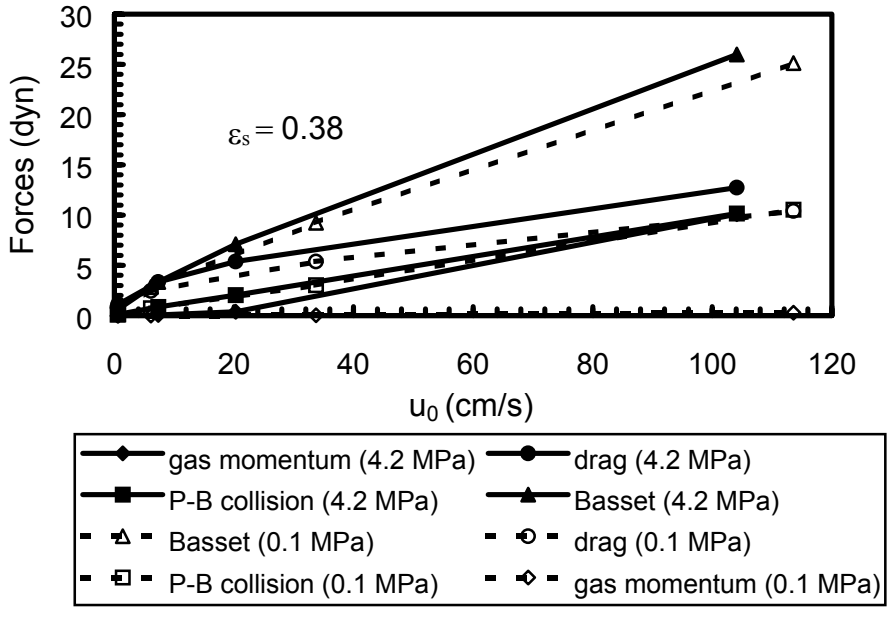

(b)

Figure 7. Effect of pressure on the various forces acting on a growing bubble.